ARTICLE **Open Access**

Vertical monolithic integration of wide- and narrow-bandgap semiconductor nanostructures on graphene films

Youngbin Tchoe[1], Janghyun Jo[2], HoSung Kim[3], Heehun Kim[1], Hyeonjun Baek[1], Keundong Lee[1], Dongha Yoo[1], Won Jun Choi[4], Miyoung Kim[2] and Gyu-Chul Yi[1]

Abstract
We report monolithic integration of indium arsenide (InAs) nanorods and zinc oxide (ZnO) nanotubes using a multilayer graphene film as a suspended substrate, and the fabrication of dual-wavelength photodetectors with the hybrid configuration of these materials. For the hybrid nanostructures, ZnO nanotubes and InAs nanorods were grown vertically on the top and bottom surfaces of the graphene films by metal-organic vapor-phase epitaxy and molecular beam epitaxy, respectively. The structural, optical, and electrical characteristics of the hybrid nanostructures were investigated using transmission electron microscopy, spectral photoresponse analysis, and current–voltage measurements. Furthermore, the hybrid nanostructures were used to fabricate dual-wavelength photodetectors sensitive to both ultraviolet and mid-infrared wavelengths.

Introduction

The monolithic integration of wide-bandgap and narrow-bandgap semiconductors is of great interest, since it broadens the spectral absorption range of light-harvesting devices and photodetectors[1–4]. Additionally, the unique properties of each material in the integrated system can be synergistically combined to create multifunctional devices. Along this line of research, many state-of-the-art tandem solar cells and photodetectors have been produced under various combinations of Si, II–VI, and III–V semiconductors[5–7], quantum dots[8], quantum wells[9], two-dimensional materials[10], and, more recently, perovskite[11] and organic materials[12]. However, the integration of wide-bandgap and narrow-bandgap semiconductors via the direct growth approach has presented a significant challenge, since heteroepitaxy works well only between two semiconductor layers with small differences between their lattice parameters and thermal expansion coefficients[13,14]. Although wafer bonding can be used to glue two different semiconductors together[15–17], the high-quality semiconductor heterostructures with a defect-free and clean interface required for many sophisticated device applications can generally only be prepared by direct growth based on heteroepitaxy[18,19]. In this work, to demonstrate monolithic integration of narrow-bandgap and wide-bandgap semiconductors, we report the growth of indium arsenide (InAs) nanorods and zinc oxide (ZnO) nanotubes on the top and bottom surfaces of a suspended graphene film. Furthermore, the hybrid nanostructures were used to fabricate dual-wavelength photodetectors sensitive to both ultraviolet and mid-infrared wavelengths. Our technique for integrating wide-bandgap and narrow-bandgap semiconductors is expected to greatly increase the versatility and power of these building blocks for applications in optoelectronics and photonics.

Correspondence: Gyu-Chul Yi (gcyi@snu.ac.kr)
[1]Department of Physics and Astronomy, Institute of Applied Physics, and Research Institute of Advanced Materials, Seoul National University, Seoul, Korea
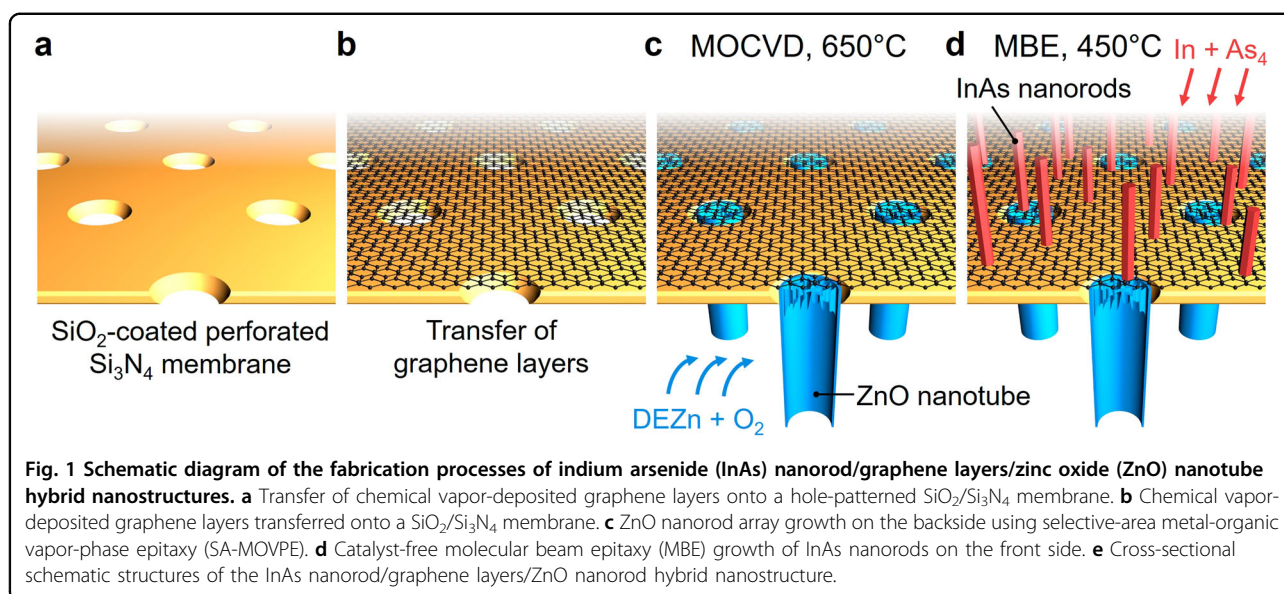[2]Department of Material Science and Engineering and Research Institute of Advanced Materials, Seoul National University, Seoul, Korea
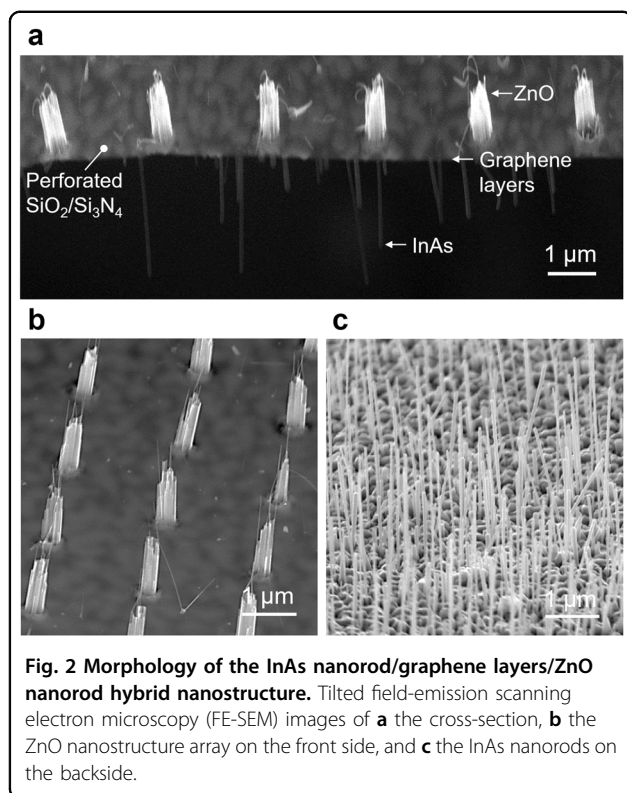Full list of author information is available at the end of the article

Fig. 1 Schematic diagram of the fabrication processes of indium arsenide (InAs) nanorod/graphene layers/zinc oxide (ZnO) nanotube hybrid nanostructures. a Transfer of chemical vapor-deposited graphene layers onto a hole-patterned SiO_2/Si_3N_4 membrane. **b** Chemical vapor-deposited graphene layers transferred onto a SiO_2/Si_3N_4 membrane. **c** ZnO nanorod array growth on the backside using selective-area metal-organic vapor-phase epitaxy (SA-MOVPE). **d** Catalyst-free molecular beam epitaxy (MBE) growth of InAs nanorods on the front side. **e** Cross-sectional schematic structures of the InAs nanorod/graphene layers/ZnO nanorod hybrid nanostructure.

Results and discussion

The basic approach for growing InAs nanorods and ZnO nanotubes on the top and bottom surfaces of suspended graphene layers and the detailed fabrication steps are schematically illustrated in Fig. 1. Suspended multilayer graphene (MLG, $n = 10$) with full coverage was synthesized by chemical vapor deposition (CVD) and transferred onto perforated silicon dioxide (SiO_2)-coated silicon nitride (Si_3N_4) membranes with 300-nm-diameter hole arrays (see Fig. 1a, b). The SiO_2/Si_3N_4 membrane with small hole openings ensured mechanically stable and flat preparation of suspended graphene layers over a relatively large area[20], while minimizing the potential for mechanical damage such as cracks or tears. The suspended graphene substrate was loaded upside down into a metal-organic chemical vapor deposition (MOCVD) system for growth of ZnO nanotubes. In this configuration, the perforated SiO_2/Si_3N_4 membrane masked the graphene layers from the reactants, and vertical ZnO nanotubes were grown at 650 °C by selective-area metal-organic vapor-phase epitaxy (SA-MOVPE), as shown in Fig. 1c. This selective-area growth is attributed to the preferred nucleation and crystal growth of ZnO at step edges on graphene films[21] and weaker interaction of Zn adatoms with the amorphous SiO_2 surface, which leads to higher desorption rate and diffusion of Zn adatoms on SiO_2 compared to those on the graphene film[22,23]. Figure 1c also schematically illustrates the existence of ZnO nanowall structures inside the nanotubes, which are usually observed for selective-area-grown ZnO nanotubes with diameters of a few hundred nanometers[22]. After the ZnO nanotubes were grown on one side of the graphene layers, the substrate was inverted to expose the other side and loaded into a molecular beam epitaxy (MBE) system.

Since the ZnO nanotubes were grown inside the 300 μm recessed cavities in the Si substrate, the sample loading and unloading process did not physically damage the ZnO nanotubes. In the MBE system, vertical InAs nanorods were grown on the opposite side of the graphene layers using a catalyst-free growth method, enabling monolithic integration of ZnO nanotubes and InAs nanorods on the suspended graphene film, as shown in Fig. 1d.

The morphologies of the InAs nanorods and ZnO nanotubes grown on each surface of the graphene layers were investigated using scanning electron microscopy (SEM). Figure 2a shows an SEM image of free-standing ZnO/MLG/InAs hybrid nanostructures, revealing the formation of ZnO nanotubes and InAs nanorods on the top and bottom surfaces of the graphene layers. Both the ZnO nanotubes and InAs nanorods were vertically well aligned on their respective surfaces on the suspended graphene layers. As shown in Fig. 2b, it is evident that ZnO nanotubes were selectively grown only on the graphene layers through the SiO_2/Si_3N_4 membrane growth mask. The diameter, spacing, and length of the ZnO nanotubes were 0.3, 2, and 3 μm, respectively. The dimensions of the ZnO nanotubes could easily be controlled by changing the diameter and spacing of the hole arrays and the growth time of ZnO. On the other side of the graphene film, as shown in Fig. 2c, high-density vertical InAs nanorods with an average length of 3 μm, a diameter of 50 nm, and a density of 5 μm^{-1} were formed. SEM images showed that the density of the InAs nanorods was uniform across the graphene layers and was not affected by the presence of the ZnO nanotubes grown on the other side. This observation suggests that the MLG ($n = 10$) screened the interaction[19] between the two different semiconductors, and that the nucleation of the

Fig. 2 Morphology of the InAs nanorod/graphene layers/ZnO nanorod hybrid nanostructure. Tilted field-emission scanning electron microscopy (FE-SEM) images of **a** the cross-section, **b** the ZnO nanostructure array on the front side, and **c** the InAs nanorods on the backside.

InAs nanorods was not affected by the ZnO nanotubes grown on the other side.

In addition to the ZnO/MLG/InAs heterostructures, we also demonstrated gallium nitride (GaN) microrod/MLG/InAs heterostructures using the same integration strategy (see Fig. S1). The GaN microrods grown on graphene layers[24] were transferred onto a Si substrate with 300 × 300 μm^2 square window openings; the sample was loaded upside down into the MBE system, and InAs nanorods were grown on the back side of the exposed graphene layers. The SEM image in Fig. S1 reveals that InAs nanorods and GaN microrods were vertically integrated through the thin graphene layers. In this work, the integration of ZnO nanotubes or GaN microrods with InAs nanorods is presented as a representative example, since these materials are difficult to integrate using conventional growth approaches due to the very large differences in their physical characteristics. Although only two combinations were demonstrated in this work, we strongly believe that a greater variety of materials can be monolithically integrated using the same approach.

The microstructural characteristics of the InAs/MLG/ZnO hybrid nanostructures were investigated using transmission electron microscopy (TEM). The bright-field (BF) cross-sectional TEM in Fig. 3a clearly shows an integrated structure composed of ZnO nanotubes with nanowalls vertically grown on top of the MLG through the SiO_2/Si_3N_4 membrane, and InAs nanorods and

nanoislands grown on the opposite side of the MLG. The atomic arrangement and interfacial layers between the hybrid InAs/MLG/ZnO layers were also examined using high-resolution TEM (HR-TEM), as shown in Fig. 3b. The HR-TEM image clearly indicates that the InAs nanorods and ZnO nanotubes were grown as single crystals on each side of the MLG without any interfacial layers or gaps. The lattice spacings between adjacent planes were estimated to be 0.26, 0.34, and 0.35 nm, corresponding to the *d*-spacings of ZnO(0002), graphene layers(0002), and InAs(111) planes[22,25]. Additionally, compositional analysis conducted using scanning TEM (STEM) equipped with an energy dispersive X-ray spectroscopy system (Fig. S2) showed that there was no interdiffusion through the interface layers, and that the graphene films effectively prevented In and As_4 fluxes from passing through to the other side of the graphene layers during growth.

The crystallinity of the heterostructure was further investigated by analyzing diffraction patterns (DPs) with a selective aperture size of 150 nm. Figure 3c−e show the DPs from the ZnO nanotubes, InAs nanorods, and ZnO/MLG/InAs interfaces, respectively. The DPs in Fig. 3c, d were measured along the zone axis near the $[2\bar{1}10]$ direction of ZnO and $[11\bar{2}0]_{WZ}$ and $[1\bar{1}0]_{ZB}$ directions of InAs, respectively. The patterns revealed that ZnO nanotubes with a wurtzite single crystal structure and a *c*-axis orientation grew normal to the graphene layers. On the other hand, streak patterns were observed in the DP of the InAs nanorods as a result of the stacking faults typically observed in InAs nanorods[25,26]. The InAs nanorods exhibited $(111)_{ZB}$ and $(0002)_{WZ}$ orientations normal to the graphene. The DP near the ZnO/MLG/InAs interfaces showed diffraction peaks of ZnO and InAs that were exactly the same as those in the overlapped DPs of crystalline ZnO and InAs shown in Fig. 3c, d, respectively. In addition to the DP analysis, the fast Fourier transform of the HR-TEM image (see Fig. S3) revealed the alignment of the C(0002) peak with the ZnO(0002) and InAs$(111)_{ZB}$, $(0002)_{WZ}$ peaks. This result indicates that the ZnO nanotubes and InAs nanorods were heteroepitaxially grown on graphene layers with an epitaxial relationship of InAs$(111)_{ZB}$,$(0002)_{WZ}$ || MLG(0002) || ZnO(0002).

The in-plane epitaxial relationships among the InAs nanorods, MLG, and ZnO nanotubes were investigated by plan-view TEM. For these experiments, we prepared InAs/MLG/ZnO hybrid heterostructures on graphene layers with nanoscale ZnO and InAs nuclei, which are small enough for electron beam transmission. These nuclei were grown on graphene layers for a very short time such that their average sizes were controlled to be less than 50 nm, and the suspended graphene layers were electron beam transparent. Figure 3f shows a plan-view HR-TEM image of the hybrid heterostructure near the point of intersection of InAs, MLG, and ZnO single
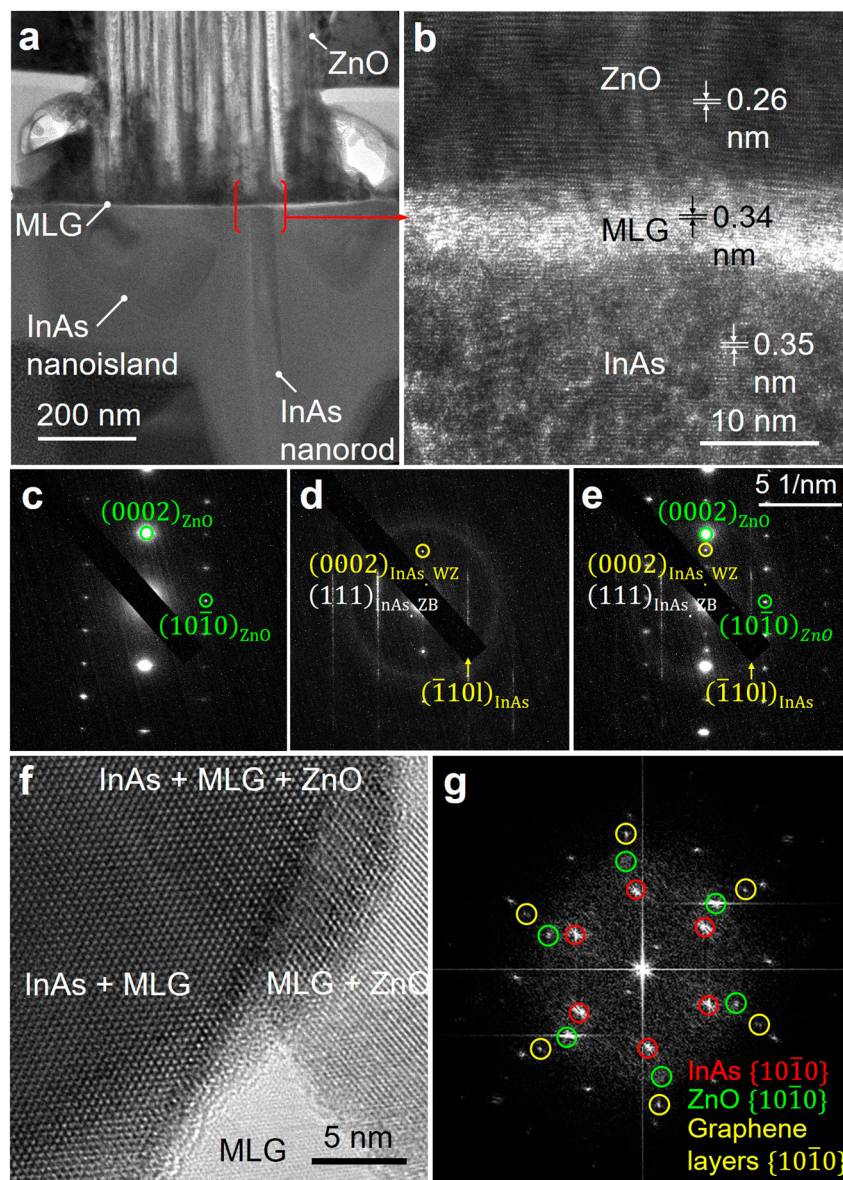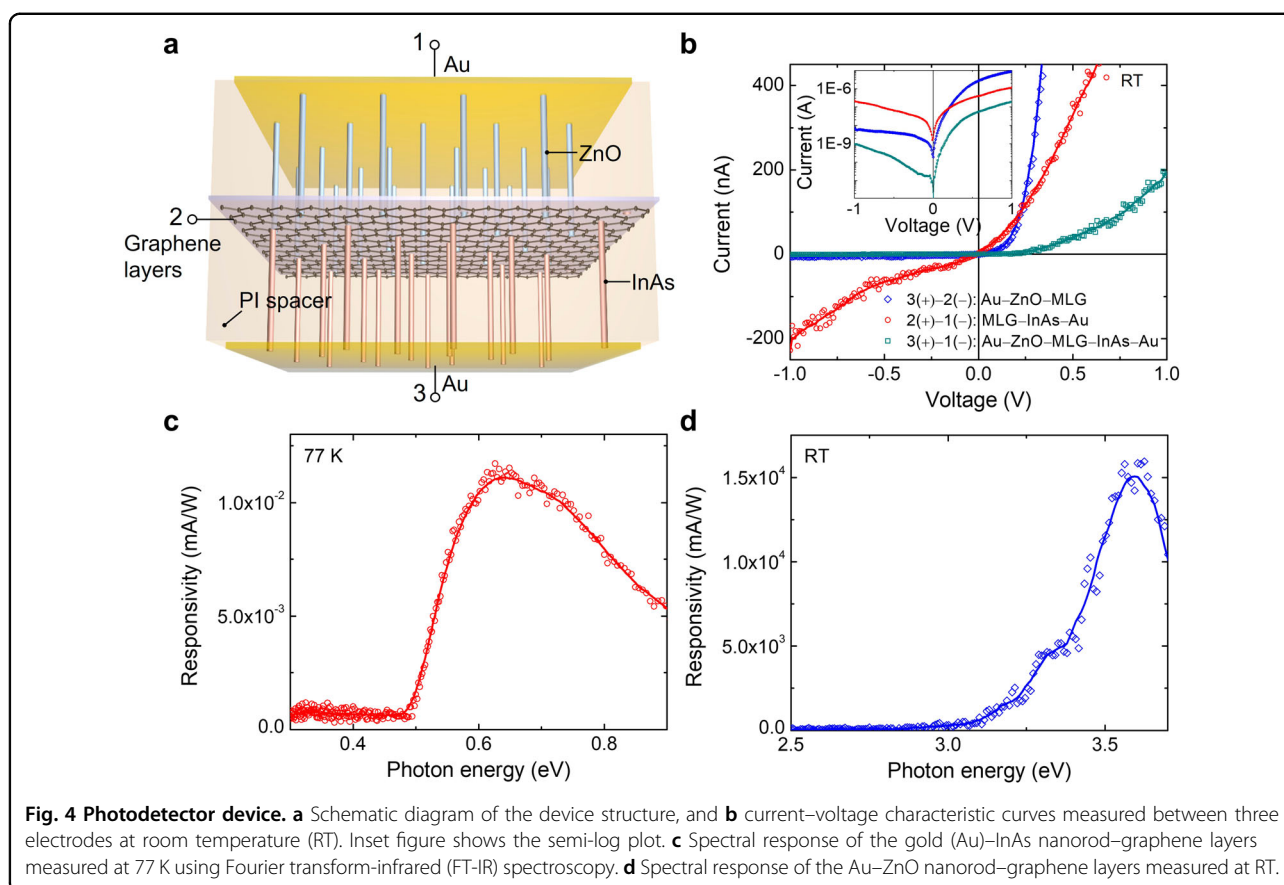
Fig. 3 Cross-sectional transmission electron microscopy (TEM) analysis of the hybrid heterostructure. a Bright-field and **b** high-resolution (HR)-TEM images of the hybrid heterostructures near the ZnO nanorod/multilayer graphene (MLG)/InAs nanorod interfaces. Diffraction patterns acquired using a selective aperture size of 150 nm near the **c** ZnO nanorod, **d** InAs nanorod, and **e** ZnO/MLG/InAs interfaces. Plan-view TEM structural analysis of the heterostructure. **f** Plan-view HR-TEM image showing overlap of InAs and ZnO nuclei. **g** Corresponding fast Fourier transform of **f**.

crystals; the hexagonal lattice structures of InAs, ZnO, and MLG are clearly visible in this HR-TEM image. On the upper side of the HR-TEM image, all three crystals, InAs/MLG/ZnO, overlapped, while on the left or right side of the image, two crystals (either InAs/MLG or MLG/ZnO) overlapped. There were no overlapping semiconductor crystals on the lower side of the HR-TEM image where only the periodic lattice structure of MLG is observed. We analyzed the fast Fourier transform (FFT) (see Fig. 3g) of the HR-TEM image to determine the in-plane orientations of InAs, ZnO, and MLG and confirmed

that both the ZnO and InAs nanostructures were grown heteroepitaxially on the graphene layers with an in-plane heteroepitaxial relationship of InAs $(10\bar{1}0)$ || MLG $(10\bar{1}0)$|| ZnO$(10\bar{1}0)$. These results again suggest that graphene film could be an excellent heteroepitaxial substrate to integrate many different semiconductor crystals.

A vertical photodetector was fabricated as a representative example of a device application using the InAs nanorod/MLG/ZnO nanotube hybrid heterostructures. Figure 4a schematically illustrates the device structure, where gold (Au) electrodes, as Schottky contacts, were

Fig. 4 Photodetector device. a Schematic diagram of the device structure, and **b** current–voltage characteristic curves measured between three electrodes at room temperature (RT). Inset figure shows the semi-log plot. **c** Spectral response of the gold (Au)–InAs nanorod–graphene layers measured at 77 K using Fourier transform-infrared (FT-IR) spectroscopy. **d** Spectral response of the Au–ZnO nanorod–graphene layers measured at RT.

formed on the tips of the InAs nanorods and ZnO nanotubes, and silver paste provided ohmic contact to the CVD-graphene layers. For electrical isolation between the electrodes, 2-μm-thick polyimide (PI) layers were formed as spacers on both the top and bottom sides of the graphene layers, and oxygen plasma etching was performed to selectively expose the tips of the InAs and ZnO nanorods (see Fig. S4).

The current–voltage ($I–V$) characteristic curves between the three electrodes are shown in Fig. 4b. Schottky diode characteristics with clear rectifying behavior were observed for the $I–V$ curve measured for the Au–ZnO nanotube–MLG device. This is expected, as Au and ZnO nanotubes are capable of forming high-quality Schottky contacts[27], and ZnO nanotubes grown on graphene layers form ohmic contacts with the graphene layers[22]. Meanwhile, the $I–V$ curve for the Au–InAs nanorod–MLG device was nonlinear, as is the curve typical for two-terminal devices with Schottky contacts on both sides; slightly higher current levels were observed at forward bias voltages. This observation agrees with previous results, in which InAs nanorods generally exhibited a higher Schottky barrier for a metal contact with a lower work function; the work functions of the Au and graphene layers are 5.2 and 4.5 eV, respectively[28,29]. The $I–V$

curves of the Au–InAs nanorod–MLG device measured at 10 K (Fig. S5) showed clear rectifying behavior with suppression of a large thermionic current typical for narrow-bandgap semiconductor-based devices. The $I–V$ characteristic curve for the Au–ZnO–MLG – InAs–Au device appeared as if the above two devices were connected in series; the overall resistance of each system was additive, and clear rectifying behavior was observed based on the dominance of the Au–ZnO Schottky contact.

We measured the spectral responsivity of the Schottky photodiodes to determine the spectral absorption range of the hybrid photodiode. As shown in Fig. 4c, the spectral response of the InAs nanorod-side device (Au–InAs–MLG) generated a photocurrent above a photon energy of 0.5 eV, and the peak responsivity was observed near 0.6 eV, similar to previously reported values[30]. Meanwhile, the spectral response of the ZnO nanotube-side Schottky photodiode (Au–ZnO–MLG) showed that a photocurrent was observed above a photon energy of 3.1 eV, and the responsivity peaked near 3.6 eV (Fig. 4d). The cutoff energy was close to 3.1 eV, which is similar to previously reported values[31], and indicates the selective spectral sensitivity of ZnO nanorod devices to UV light. Although we characterized the mid-IR photodetector characteristics of the InAs nanorod-side device with the

InAs side facing up because of the sampling loading protocol of the FT-IR system, we expect the device to work equivalently well with the ZnO side facing up due to the mid-IR transparency of both ZnO[32] and graphene layers[33]. These results strongly suggest that the device made with these hybrid heterostructures, composed of wide-bandgap and narrow-bandgap semiconductor nanorods integrated on graphene layers, can monolithically combine each material's unique optoelectronic properties, capturing photons over a wide spectral range and generating photocurrents. Such characteristics are highly desirable for broadband light-harvesting device applications.

In conclusion, we demonstrated monolithic heteroepitaxial growth of single-crystalline wide-bandgap and narrow-bandgap semiconductor nanostructures on the top and bottom surfaces of graphene layers. The graphene layers provided vertical alignment and a heteroepitaxial relationship to both InAs nanorods and ZnO nanotubes. Cross-sectional and plan-view TEM analyses directly showed the heteroepitaxial relationship in the ZnO nanotube/graphene layers/InAs nanorod hybrid heterostructure. Moreover, dual-wavelength photodetectors were fabricated using these hybrid heterostructures, and a clear optoelectronic response to UV and mid-IR light was observed. We believe that this general approach of combining various semiconductor nanostructures can be applied to many other hybrid nanostructures with unique physical properties that can be used for advanced optoelectronic device applications, such as tandem cells or multicolor light emitters.

Experimental methods
Preparation of graphene layers

Graphene films were deposited on Cu foil using CVD and spin-coated with PMMA. The PMMA-supported graphene was transferred onto a hole-patterned SiO_2/ Si_3N_4 membrane, and the PMMA layer was removed by organic solvents. The hole-patterned SiO_2/Si_3N_4 membrane was prepared by anisotropic wet etching of a Si_3N_4-coated Si wafer, hole patterning by electron beam lithography, dry etching, and plasma-enhanced CVD of a 50-nm-thick SiO_2 layer on the hole-patterned Si_3N_4 membrane. Raman spectroscopy and cross-sectional TEM confirmed the successful preparation of graphene layers and their layer number ($n = 10$).

Selective-area metal-organic vapor-phase epitaxy of ZnO nanorods on graphene layers

ZnO nanotubes were selectively grown on graphene layers using catalyst-free MOVPE. Diethylzinc (DEZn) and high-purity O_2 (>99.9999%) were used as reactants, and high-purity Ar (>99.9999%) was the carrier gas. The flow rates of DEZn and O_2 were 30 and 90 sccm, respectively. During growth, Ar flowed into the quartz reactor through a DEZn bubbler held at $-15\,°C$. To prevent premature reaction, the O_2 gas line was separated from the main gas manifold line. The reactor pressure was kept at 0.3 Torr during growth, and the temperature was 650 °C. More details on the experimental setup of the MOVPE growth system can be found elsewhere[12].

Molecular beam epitaxial growth of InAs nanorods on graphene layers

Inside of a cryogenically cooled ultrahigh-vacuum growth chamber (RIBER 32P), InAs nanorods were grown at 450 °C for 35 min by supplying high-purity In and uncracked arsenic (As_4) molecular beams from Knudsen cells. The beam-equivalent pressures of In and As_4 were 1×10^{-7} and 3×10^{-5} Torr, respectively. For catalyst-free growth of InAs nanorods, we supplied As_4 to the substrates for 10 min before supplying In to prevent In droplet formation on the graphene layers. More details of the experimental setup of the MBE growth system can be found elsewhere[34].

Surface morphology and microstructural characterization

The morphology of the ZnO nanorod/graphene layers/ InAs nanorod hybrid heterostructure was investigated using FE-SEM (MIRA3; TESCAN and AURIGA; Carl Zeiss). For detailed microstructural analysis, the cross-section was prepared by dual-beam FIB (Quanta 3D; FEG) and analyzed using TEM (Tecnai F20; FEI). The chemical composition was analyzed by high-angle annular dark-field STEM-EDX (JEM 2100F; JEOL). The plan-view TEM specimen was prepared by growing nanoscale ZnO and InAs nuclei on each side of the graphene layers. ZnO nuclei were grown only for 2 min, and InAs nuclei were grown for 30 s. The crystallinity of the hybrid heterostructure was investigated by BF and HR-TEM.

Vertical device fabrication

The vertical photodetector device was fabricated using InAs nanorod/graphene layers/ZnO nanorod hybrid heterostructures. Prior to metallization, PI layers were coated on both sides of the InAs/MLG/ZnO structure, and oxygen plasma was used to expose the tips of the ZnO and InAs nanorods through the PI layers. Gold electrodes with thicknesses of 20 and 50 nm were deposited on the ZnO and InAs nanorods, respectively. The transmittance of the 20-nm-thick Au layer at 300 nm was estimated to be 20%, and that of the 50-nm-thick Au layer at 2500 nm was estimated to be 0.2%[35,36]. Silver paste was used to provide ohmic contact to the CVD-graphene layers[37], which was confirmed by two-probe measurements.

Photodetector characterization

The spectral response of the ZnO nanorod/graphene layers photodetector was measured by recording the photocurrent as a function of wavelength for monochromatic light irradiated on the device. Tunable-wavelength

monochromatic light was generated by a 300-W xenon lamp and a monochromator (DW150i; Dongwoo Optron), and the spectral power of the monochromatic light was recorded by a Si photodetector (S120VC; Thorlabs). The spectral response of the InAs nanorod/graphene layers photodetector was measured at 77 K using FT-IR spectroscopy (VERTEX 80v; Bruker), and the photocurrent was detected by a low-noise current amplifier (Keithley 428). In the FT-IR system, Globar was used as an infrared light source, together with a KBr beam splitter. An InAsSb photodetector (P13894-011NA; Hamamatsu) was used to measure the spectral intensity of the light source.

Author details
[1]Department of Physics and Astronomy, Institute of Applied Physics, and Research Institute of Advanced Materials, Seoul National University, Seoul, Korea. [2]Department of Material Science and Engineering and Research Institute of Advanced Materials, Seoul National University, Seoul, Korea. [3]Photonic/Wireless Devices Research Division, Electronics and Telecommunications Research Institute, Daejeon, Korea. [4]Center for OptoElectronic Materials and Devices, Korea Institute of Science and Technology (KIST), Seoul, Korea

Conflict of interest
The authors declare no competing interests.

Publisher's note
Springer Nature remains neutral with regard to jurisdictional claims in published maps and institutional affiliations.

References
1. Chen, R. et al. Nanolasers grown on silicon. *Nat. Photonics* **5**, 170–175 (2011).
2. Yu, G. & Lieber, C. M. Assembly and integration of semiconductor nanowires for functional nanosystems. *Pure Appl. Chem.* **82**, 2295–2314 (2010).
3. Mazid Munshi, A. & Weman, H. Advances in semiconductor nanowire growth on graphene. *Phys. Status Solidi Rapid Res. Lett.* **7**, 713–726 (2013).
4. Wang, S., Ren, Z., Guo, Y. & Gao, P. X. Nano-array integrated monolithic devices: toward rational materials design and multi-functional performance by scalable nanostructures assembly. *CrystEngComm* **18**, 2980–2993 (2016).
5. Sarkar, S. & Basak, D. Self powered highly enhanced dual wavelength ZnO@CdS core-shell nanorod arrays photodetector: an intelligent pair. *ACS Appl. Mater. Interfaces* **7**, 16322–16329 (2015).
6. Tamboli, A. C. et al. Low-cost CdTe/silicon tandem solar cells. *IEEE J. Photovolt.* **7**, 1767–1772 (2017).
7. Geisz, J. F. et al. Building a six-junction inverted metamorphic concentrator Solar. *Cell. IEEE J. Photovolt.* **8**, 626–632 (2018).
8. Semonin, O. E. et al. Peak external photocurrent quantum efficiency exceeding 100% via MEG in a quantum dot solar cell. *Science* **334**, 1530–1534 (2011).
9. Adams, J. G. J. et al. Recent results for single-junction and tandem quantum well solar cells. *Prog. Photovolt. Res. Appl.* **19**, 865–877 (2011).
10. Shi, E. et al. Colloidal antireflection coating improves graphene-silicon solar cells. *Nano Lett.* **13**, 1776–1781 (2013).
11. Choi, I. Y. et al. Two-terminal mechanical perovskite/silicon tandem solar cells with transparent conductive adhesives. *Nano Energy* **65**, 104044 (2019).
12. Wang, Y. et al. Stacked dual-wavelength near-infrared organic photodetectors. *Adv. Opt. Mater.* **28**, 1–8 (2020).
13. Vesselinov, M. I. *Crystal Growth for Beginners: Fundamentals of Nucleation, Crystal Growth and Epitaxy* (World Scientific, 2016).
14. Ayers, J. E., Kujofsa, T., Rago, P. & Raphael, J. *Heteroepitaxy of Semiconductors: Theory, Growth, and Characterization.* (CRC Press, 2016).
15. Lee, K. H. et al. Integration of GaAs, GaN, and Si-CMOS on a common 200mm Si substrate through multilayer transfer process. *Appl. Phys. Express* **9**, 086501 (2016).
16. Tanabe, K., Watanabe, K. & Arakawa, Y. III-V/Si hybrid photonic devices by direct fusion bonding. *Sci. Rep.* **2**, 1–6 (2012).
17. Jain, N. & Hudait, M. K. III–V Multijunction solar cell integration with silicon: present status, challenges and future outlook. *Energy Harvest. Syst.* **1**, 121–145 (2014).
18. Nakamura, S. GaN growth using GaN buffer layer. *Jpn J. Appl. Phys.* **30**, L1705 (1991).
19. Kim, Y. et al. Remote epitaxy through graphene enables two-dimensional material-based layer transfer. *Nature* **544**, 340–343 (2017).
20. Reina, A. et al. Large area, few-layer graphene films on arbitrary substrates by chemical vapor deposition. *Nano Lett.* **9**, 30–35 (2008).
21. Kim, Y.-J., Lee, J.-H. & Yi, G.-C. Vertically aligned ZnO nanostructures grown on graphene layers. *Appl. Phys. Lett.* **95**, 213101 (2009).
22. Kim, Y. et al. Position-and morphology-controlled ZnO nanostructures grown on graphene layers. *Adv. Mater.* **24**, 5565–5569 (2012).
23. Gačević, Ž., Gómez Sánchez, D. & Calleja, E. Formation mechanisms of gan nanowires grown by selective area growth homoepitaxy. *Nano Lett.* **15**, 1117–1121 (2015).
24. Chung, K. et al. Growth and characterizations of GaN micro-rods on graphene films for flexible light emitting diodes. *APL Mater.* **2**, 092512 (2014).
25. Hong, Y. J. et al. Van der Waals epitaxial double heterostructure: InAs/single-layer graphene/InAs. *Adv. Mater.* **25**, 6847–6853 (2013).
26. Koblmüller, G. & Abstreiter, G. Growth and properties of InGaAs nanowires on silicon. *Phys. Status Solidi Rapid Res. Lett.* **8**, 11–30 (2014).
27. Park, W. I., Yi, G.-C., Kim, J.-W. & Park, S.-M. Schottky nanocontacts on ZnO nanorod arrays. *Appl. Phys. Lett.* **82**, 4358–4360 (2003).
28. Feng, B. et al. Schottky barrier heights at the interfaces between pure-phase InAs nanowires and metal contacts. *J. Appl. Phys.* **119**, 054304 (2016).
29. Miao, J. et al. High-responsivity graphene/InAs nanowire heterojunction near-infrared photodetectors with distinct photocurrent on/off ratios. *Small* **11**, 936–942 (2015).
30. Wook Shin, H. et al. Short-wavelength infrared photodetector on Si employing strain-induced growth of very tall InAs nanowire arrays. *Sci. Rep.* **5**, 1–8 (2015).
31. Kind, H., Yan, H., Messer, B., Law, M. & Yang, P. Nanowire ultraviolet photodetectors and optical switches. *Adv. Mater.* **14**, 158 (2002).
32. Muth, J. F., Kolbas, R. M., Sharma, A. K., Oktyabrsky, S. & Narayan, J. Excitonic structure and absorption coefficient measurements of ZnO single crystal epitaxial films deposited by pulsed laser deposition. *J. Appl. Phys.* **85**, 7884–7887 (1999).
33. Adhikari, S. et al. Determining the Fermi level by absorption quenching of monolayer graphene by charge transfer doping. *Nanoscale* **8**, 18710–18717 (2016).
34. Tchoe, Y., Jo, J., Kim, M. & Yi, G. -C. Catalyst-free growth of InAs/In$_x$Ga$_{1-x}$As coaxial nanorod heterostructures on graphene layers using molecular beam epitaxy. *NPG Asia Mater* **7**, e206–e206 (2015).
35. Patoka, P. & Giersig, M. Self-assembly of latex particles for the creation of nanostructures with tunable plasmonic properties. *J. Mater. Chem.* **21**, 16783–16796 (2011).
36. Behera, G. & Ramakrishna, S. A. Enhanced broadband transmission through structured plasmonic thin films for transparent electrodes. *J. Nanophotonics* **8**, 083889 (2014).
37. Bae, S. et al. Roll-to-roll production of 30-inch graphene films for transparent electrodes. *Nat. Nanotechnol.* **5**, 574–578 (2010).